Nanometre resolution of silica hydrogel formation using time-resolved fluorescence anisotropy

C.D. Geddes, D.J.S. Birch *

Photophysics Group, Department of Physics and Applied Physics, John Anderson Building, Strathclyde University, 107 Rottenrow, Glasgow G4 0NG, Scotland, UK

Abstract

We report a new approach to particle size measurement in sol–gels which is based on fluorescence anisotropy decay. The effect of siloxane polymerisation on silica particle size and microviscosity as a function pH and sodium silicate concentration is described from initial mixing with sulphuric acid to beyond the time to the macroscopic gel point, t_g. The decay of near infra-red fluorescence anisotropy of a dye probe molecule is interpreted in terms of two rotational correlation times corresponding to solvated unbound dye and dye bound to silica particles. As polymerisation proceeds, increasing take-up of the dye from the liquid phase onto silica particles occurs. Silica primary particles of maximum mean hydrodynamic radius ≈ 1.5 nm are found to be present within the first 20 min of mixing. At pH between 1 and 0.8, irrespective of t_g, the particle size increases to a maximum radius of ≈ 4.5 nm after ≈ 2000 min. Lowering the pH in the range 0.8–0.15 produces a maximum radius of ≈ 3.5 nm. For all the sols studied, intra-particle syneresis then reduces the final particle radius by ≈ 0.5 nm within ≈ 6000 min. Although the bulk properties of the sol–gel change drastically at t_g, the probe detects little change in the microviscosity. © 2000 Elsevier Science B.V. All rights reserved.

1. Introduction

The sol–gel process enables the production of glasses at room temperature and has its origins in the pioneering work of Graham and Ebelman in the 19th century [1]. The process for producing silica gel is well understood at the manufacturing level and involves mixing sulphuric acid and an aqueous solution of sodium silicate under controlled conditions to form a sol and eventually a hydrogel. The time to gelation is defined in terms of a macroscopic gel point, t_g, at which a fine silica network spans the containing vessel. Applications of silica gel are multifarious and include cleaning, polishing, liquor refining, printing, adhesives and paints to name but a few. More recently, silica alcogels made from silicon alkoxides (e.g., tetramethyl or tetraethyl orthosilicate) in alcohol solutions have been the subject of research interest for new optical applications. Ease of moulding, graded refractive index capabilities and a shorter wavelength of transmission than silica fused at high temperature are a few of the reasons for this. Moreover, because of their ease of forming an optically clear glass, even when doped with high concentrations of aromatic dyes, sol–gel glasses make excellent fluorescent matrices for use as laser

---

* Corresponding author. Tel.: +44-141 548 3377; fax: +44-141 552 2891.

E-mail address: djs.birch@strath.ac.uk (D.J.S. Birch).

gain media, solar collectors, nonlinear optical components and sensors [2].

The end product of a rigid network of siloxane (–Si–O–Si–) bonds is essentially the same for both hydrogels and alcogels. Nevertheless, a better understanding of how factors such as viscosity, pH, temperature, reactant concentrations, etc., influence the sol–gel kinetics at the molecular level could have benefits ranging from a better defined end product to a whole new generation of bespoke sol–gel materials. In particular, the mechanisms initiating polymerisation and aggregation in the sol and at the end as the gel contracts and dries are poorly resolved at the molecular level. Only over the past two decades has the picture emerged of silica hydrogel being formed by the coalescence of polymer particles rather than through the extension and cross-linking of polymer chains, as is the case for organic polymers [1]. The question of how the properties of the sol are 'memorised' in the gel is still very much in debate, not least of which because of the difficulty in continuously measuring particle size during the early stages of polymerisation (i.e., $\leqslant 2$ nm radius).

Fluorescence techniques based on tracking the photophysical properties of a molecular probe to indicate changes in local environment have earned a well-deserved reputation [3]. This is because fluorescence has high sensitivity (even single molecules can now be detected) and can be observed in a time frame spanning femtoseconds to microseconds, giving fluorescence the potential to resolve many physical processes, including those to be discussed here. It is thus somewhat surprising that there are few if any examples of one of the most powerful fluorescence techniques, namely anisotropy decay, being used to track changes in particle size in colloids. Indeed, as we will demonstrate here, fluorescence anisotropy is ideally suited to the study of particles in sol–gels.

Although silica alcogels have recently been studied using fluorescence probes [4,5], their acidic hydrogel counterparts are more difficult to study because of intrinsic fluorescence and low pH which frequently leads to chemical degradation of aromatic probes. We have succeeded in overcoming these problems by using the xanthene type probe, JA120 [6], which we have found to have fluorescence characteristics unperturbed by this harsh environment. The near infra-red fluorescence of this dye (spectral peak at 690 nm) brings with it additional benefits in this application in respect of reduced Rayleigh scattering of excitation and fluorescence (inverse fourth power of wavelength dependence), negligible sol–gel intrinsic fluorescence and compatibility with diode laser excitation such that polarised fluorescence decays can be measured accurately in ≈ 2 min time windows, during which time any change in the sol–gel is minimised.

Previous results on silica alcogels, using phase fluorometry to record the time-resolved anisotropy of the probe rhodamine 6G, were described by Bright et al. [5] in terms of the probe always being unbound and having two rotational times of constant fractions prior to gelation. This was interpreted as providing evidence for the coexistence of two discrete fluid microdomains of different viscosities [5]. Our pulse fluorometry results on silica hydrogels with JA120 as a probe are in some ways similar, but there are salient differences which lead us to propose a quite different interpretation in terms of one fluid domain in which silica particles are dispersed from the very early stages of polymerisation. Changes in the decay of fluorescence anisotropy as polymerisation proceeds are simply explained in terms of changes in the relative abundance of free probe and probe bound to silica particles. This dual behaviour of the probe means that a single anisotropy decay measurement leads to determination of both the fluid microviscosity and the particle size. An interesting and perhaps surprising consequence of our interpretation is the way in which the extreme differences in bulk properties between the sol and the gel are reflected only in subtle changes in the fluid dynamics on the nanometre scale.

Traditional techniques for particle size measurement in silica sols are largely based on small angle X-ray, neutron and light scattering [1]. Because fluorescence depolarisation is only caused by rotating particles, the technique we describe is better placed than traditional methods for recording particle size in situ at high silicate concentrations and after gelation.

2. Theory

The theory and application of fluorescence depolarisation has been reviewed many times for bio- and organic polymers [7–9]. We summarise the relevant parts here.

Basically, by recording vertically and horizontally polarised fluorescence decay curves, $F_V(t)$ and $F_H(t)$, orthogonal to vertically polarised excitation, an anisotropy function $R(t)$ can be generated, i.e.,

$$R(t) = \frac{F_V(t) - F_H(t)}{F_V(t) + 2F_H(t)}. \qquad (1)$$

For an unbound spherical rigid rotor in an isotropic solvent the decay of $R(t)$ which describes depolarisation of the fluorescence due to Brownian rotation can be expressed as

$$R(t) = R_0 \exp(-t/\tau_r), \qquad (2)$$

where R_0 is the initial anisotropy with a maximum value of 0.4 and, in the simplest case, τ_r is described by the Stokes–Einstein equation,

$$\tau_r = \eta V/kT, \qquad (3)$$

where η is the viscosity, V the molecular volume, T temperature and k is the Boltzmann constant.

In our case, studies of JA120 in a range of solvents of known viscosity showed it to be well described by an isotropic rotor with radius of 7.5 Å; a figure which we have used in subsequent viscosity calculations. This value is consistent with 5.8 Å and 4.8 Å found for rhodamine 700 and rhodamine 800, respectively [10]. In the case of hindered molecular rotation, such as for a fluorophore bound to a macromolecule, which rotates on a much longer time scale, or in an ordered media such as a lipid bilayer membrane in the gel phase, the fluorescence is only partially depolarised, leading to a residual anisotropy function R_∞ given by

$$R(t) = (R_0 - R_\infty)\exp(-t/\tau_r) + R_\infty. \qquad (4)$$

In this case τ_r reflects the vicinal viscosity close to the binding site, which may be markedly different from that in bulk solution described by Eq. (2).

In the model we propose here, where a fraction f of the total fluorescence is due to the probe molecules bound to silica particles and hence $1 - f$ attributed to probe molecules solvated and unbound in the sol, the anisotropy takes on the form

$$R(t) = (1 - f)R_0 \exp(-t/\tau_{r1}) + fR_0 \exp(-t/\tau_{r2}). \qquad (5)$$

Eq. (5) assumes that the fluorescence lifetimes of solvated and bound probe molecules are the same. In reality the difference is sufficiently small for Eq. (5) to provide a good description (see Section 4). Expanding $\exp(-t/\tau_{r2})$ and putting $\tau_{r1} \ll \tau_{r2}$ to reflect free probe molecules rotating much faster than those which are bound to silica particles; then in the case where the fluorescence lifetime $\tau_f \ll \tau_{r2}$, an expression of similar form, but different interpretation to Eq. (4), is obtained, namely

$$R(t) = (1 - f)R_0 \exp(-t/\tau_{r1}) + fR_0. \qquad (6)$$

We have found that Eq. (5) provides the best description of polymerisation in silica hydrogels over all times with Eqs. (2) and (6) only providing an adequate description at times well after the point of macrogelation has occurred. It should be noted that only if the fluorescence quantum yield of the probe is the same when unbound in the sol as it is when bound to silica particles, does the fraction f exactly describe the probe partition ratio between the sol and silica.

If a fraction of the fluorescence g is attributed to dye bound rigidly within a gel (and thus providing no fluorescence depolarisation) in addition to free dye in the sol and dye bound to particles, then Eq. (5) could be extended to

$$R(t) = (1 - f - g)R_0 \exp(-t/\tau_{r1}) + fR_0 \exp(-t/\tau_{r2}) + gR_0. \qquad (7)$$

However, Eq. (7) was not found to provide a good description of the anisotropy decays reported here. Visually the anisotropy was observed to decay at all but the later polymerisation times, suggesting that g is a small fraction of the total fluorescence. However, in the short measurement times used it is

likely that Eq. (7), although very plausible, cannot be supported by the statistical precision available.
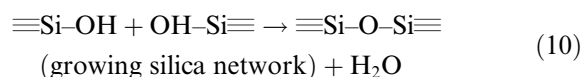
3. Materials and methods

The sol–gel process is a room temperature synthetic inorganic polymerisation, through a series of hydrolysis and condensation steps of sodium silicate solution (water glass). In the simplest case,

$$Na_2O \cdot xSiO_2 \cdot YH_2O + H_2SO_4$$
$$\rightarrow SiO_2 + Na_2SO_4 + (Y + 1)H_2O \qquad (8)$$
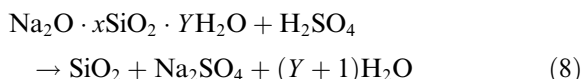
where x denotes the molar ratio of the glass; in our case $x \approx 3.3$. The first step of the process is hydrolysis (protonation)

$$Na_2O \cdot xSiO_2 \cdot H_2O + H_2SO_4$$
$$\rightarrow Si(OH)_4 + Na_2SO_4 \qquad (9)$$
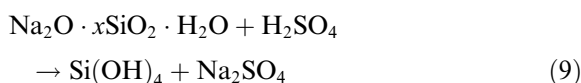
Followed by stepwise polymerisation by condensation and dehydration

$$\equiv Si\text{–}OH + OH\text{–}Si\equiv \ \rightarrow \ \equiv Si\text{–}O\text{–}Si\equiv$$
$$(\text{growing silica network}) + H_2O \qquad (10)$$

where the rate below pH 2 is proportional to $[H^+]$.

The fluorescent probe JA120, was synthesized and supplied by Dr Jutta Arden-Jacob, University of Seigen, Germany [6]. The structure of JA120 is shown in Fig. 1. 79.5 Twaddle sodium silicate (Crystal 79) (the 'twaddle' (°Tw) is a unit of density first used at the turn of the century, to enable
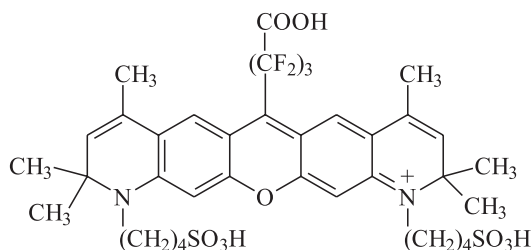

Fig. 1. The structure of the near-infrared fluorescence probe JA120.

workers to easily deal with integers and is still used as an industrial unit. SI conversion: Twaddle = 200 (density/g cm^{-3} − 1)) and 50% (specific gravity 1.4) sulphuric acid were supplied by Crosfield. Suitable acid and sodium silicate solutions (Na$_2$O · xSiO$_2$ · H$_2$O, $x \approx 3.3$) were prepared by dilution with doubly de-ionised water. The % Na$_2$O in sodium silicate solution was determined by titration with HCl (Eq. (11)), whilst the % SiO$_2$ determined by titrating the NaOH liberated from the reaction of Si(OH)$_4$ with NaF (Eq. (12)), with HCl.

$$Na_2O + 2HCl \rightarrow 2NaCl + H_2O \qquad (11)$$

$$Si(OH)_4 + 6NaF \rightarrow Na_2SiF_6 + 4NaOH \qquad (12)$$
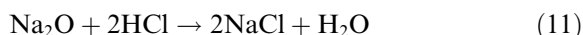
Different concentrations of sulphuric acid and silicate were mixed together using stainless steel blades rotating at 1200 rpm and delivered at controlled flow rates using peristaltic pumps to produce specific sol–gels of differing macrogelation time, t_g, as summarised in Table 1 and shown in Fig. 2. The t_g values for both Systems a and b sol–gels were determined by noting the range of times when 1 l of sol (using the same 1 l Nalgene beaker) had thickened sufficiently to start peeling away from sides of the beaker to the point when it could no longer flow and had set firm. Obviously for low density sol–gels t_g is broader and greater than for higher density (i.e., greater % w/w SiO$_2$) sol–gels containing the same excess acid normality. JA120 was added to the bulk mix to give concentrations of $\approx 5 \times 10^{-6}$ M directly after mixing and the sol then cast into 4 cm^3 plastic cuvettes (Hughes and Hughes). For the measurements described here no differences were observed in the anisotropy decay when using plastic and quartz cuvettes. The excess acid normality in final sols was determined both stoichiometrically and by acid–base titration with 1 N NaOH. Both are in very good agreement. The % SiO$_2$ in final gels was determined stoichiometrically. The polymerisation is exothermic and depending on the mixture the sol–gel temperature increases up to $\approx 10°$C, but reaches ambient within one hour. Between anisotropy measurements the sol–gels were left at room temperature in unsealed cuvettes.

Table 1
Sol–gel Systems a and b

Silicate		Acid		Flow rate (ml s^{-1})		Excess acid normality in sol–gel		Final % SiO$_2$ in sol–gel	t_g (min)
Initial %	Initial °Tw	Initial %	Initial °Tw	Silicate	Acid	N	pH		
System a									
20.21	50	34	50.2	7.58	2.43	0.27	0.87	15.30	60–74
16.94	40	28	40	7.58	2.53	0.25	0.90	12.70	240–270
12.50	30	22	30	7.25	2.66	0.31	0.81	9.14	990–1050
8.62	20	15	20	6.76	2.92	0.30	0.82	6.02	2760–3240
System b									
20.07	50	30	45	7.81	2.60	0.21	0.98	15.13	77–96
19.79	50	34	50	8.62	2.75	0.37	0.73	15.00	68–74
19.81	50	40	60	8.20	2.55	0.60	0.52	14.97	47–55
20.81	50	42	65	6.76	2.58	1.40	0.15	14.81	13–16

SI conversion: Twaddle (°Tw) = 200 (density/g cm^{-3} − 1).
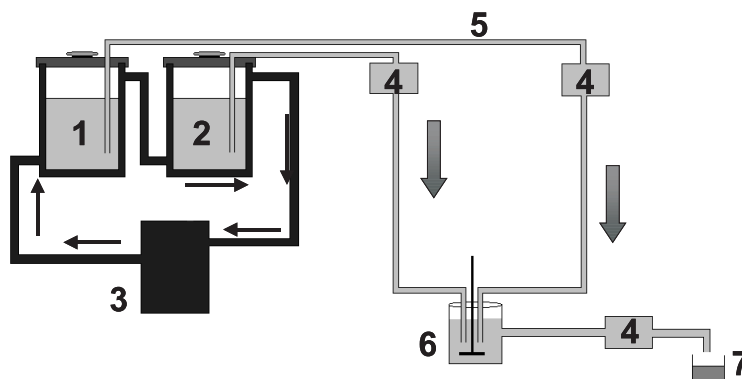

Fig. 2. Continuous flow system for the preparation of acidic hydrogels. 1 – sodium silicate solution (water glass); 2 – sulphuric acid; 3 – thermostat; 4 – peristaltic pumps; 5 – marprene tubing; 6 – mixing head vessel; 7 – sol–gel.

Orthogonal, polarised fluorescence decay kinetics were recorded using the time-correlated single-photon counting technique [9] in ≈2 min measurement times at different delay times following initial mixing of the sol, as shown in Fig. 3. This incorporated a Hamamatsu PLP-02 diode laser for excitation and an EG&G CD2027 single photon avalanche diode for detection. The 650 nm diode laser generated 70 mW vertically polarised optical pulses of duration ≈50 ps at 1 MHz repetition rate. The overall instrumental response function was ≈350 ps FWHM. Fluorescence was selected using an IBH Model 5000 M $f/3$ monochromator with a spectral range of 300–1200 nm, a Kodak 700 nm cut-off filter and a dichroic polariser (Halbro Optics). Non-linear least squares impulse reconvolution analysis of the anisotropy data [9] was performed using the IBH software. The procedure for impulse reconvolution corrects for distortion due to the finite instrumental response. This first involves fitting to the fluorescence decay given by $F_V(t) + 2F_H(t)$, (the denominator in (Eq. (1)) and obtaining the corresponding fluorescence impulse response function, $I(t)$. The product of $I(t)$ multiplied by iterations of $R(t)$ are then convoluted with the measured instrumental response function and fitted to the measured difference data (the numerator in
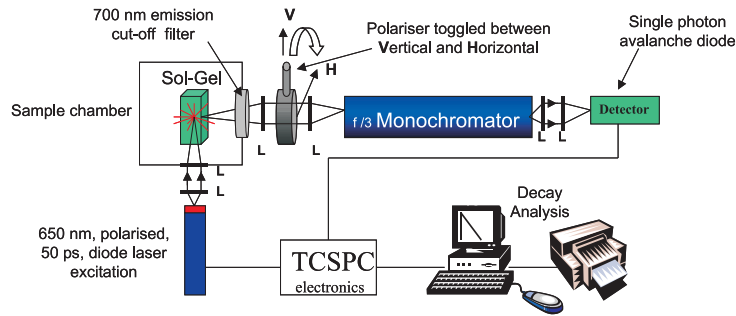
Fig. 3. Fluorescence anisotropy decay measurement of silica hydrogels using time-correlated single-photon counting. L – lenses.

Eq. (1)), $F_{v}(t) - F_{H}(t)$, using non-linear least squares, with a minimisation of chi-squared, χ^2, goodness of fit criterion. A normalised χ^2 value close to unity indicates the absence of systematic errors and an appropriate anisotropy decay model $R(t)$ described by the best fit parameters, e.g., τ_{r1}, τ_{r2}, R_0, f. For all the measurements the samples remained optically transparent such that depolarisation due to multilple scattering from particles and pores can be neglected.

4. Results

Two differing sol–gel systems have been studied as shown in Table 1. *System a* is described by a constant excess acid normality and varying % SiO_2 in the final sols and *System b* is for a constant % SiO_2 and varying acid normality in final sols. These were chosen in order to obtain more meaningful comparisons of the rates of sol–gel polymerisation rather than allowing both the % SiO_2 and excess acid normality to vary together.

Fig. 4 shows a typical data set of polarised fluorescence decays and the derived anisotropy function. Typical results of reconvolution analysis of fluorescence anisotropy data for one of the silicate/acid compositions is shown in Table 2 for the possible kinetic interpretations given by Eqs. (2), (4)/(6) and (5). Some common features of the analysis of all the compositions studied in terms of the χ^2 and goodness of fit emerge. Namely, Eq. (2) only describes the anisotropy decay at long times and Eq. (5) consistently provides a better de-

scription than Eq. (6). The former observation leads to the conclusion that not even at the outset does the sol exist as a simple solution. The question as to why Eq. (2) fits the data at long times is answered in the discussion which follows.

The anisotropy decay parameters shown in Table 2 were obtained by impulse reconvolution analysis of the difference data $F_{V}(t) - F_{H}(t)$ in the range 5000–10 000 counts; higher counts not being possible in most cases or the sol–gel might have changed significantly during the measurement. Distinguishing between the alternative kinetic models of two rotational times and zero residual anisotropy (Eq. (5)) and one rotational time and a non-zero residual anisotropy (Eqs. (4) and (6)) is not so easy to establish in a single measurement at these levels of statistical precision [11]. Indeed, the two models are not necessarily mutually exclusive because, on longer time scales than we are able to observe the anisotropy with reasonable statistical precision ($\approx$20 ns), a long rotational time could be equally well described by a residual anisotropy. This is because anisotropy information is only available during the short fluorescence decay of JA120 (lifetime in H_2O $\approx$1.83 ns). However, for the eight sol–gel systems shown in Table 1, producing in excess of 150 anisotropy decays, fitting to Eq. (5) consistently gave a lower chi-squared value than Eq. (6). Moreover, increasing the complexity to two rotational times and a residual anisotropy (Eq. (7)) to reflect the additional possibility of significant fluorescence from dye bound rigidly in a silica matrix, produced evidence of over-parameterisation, e.g., physically meaningless
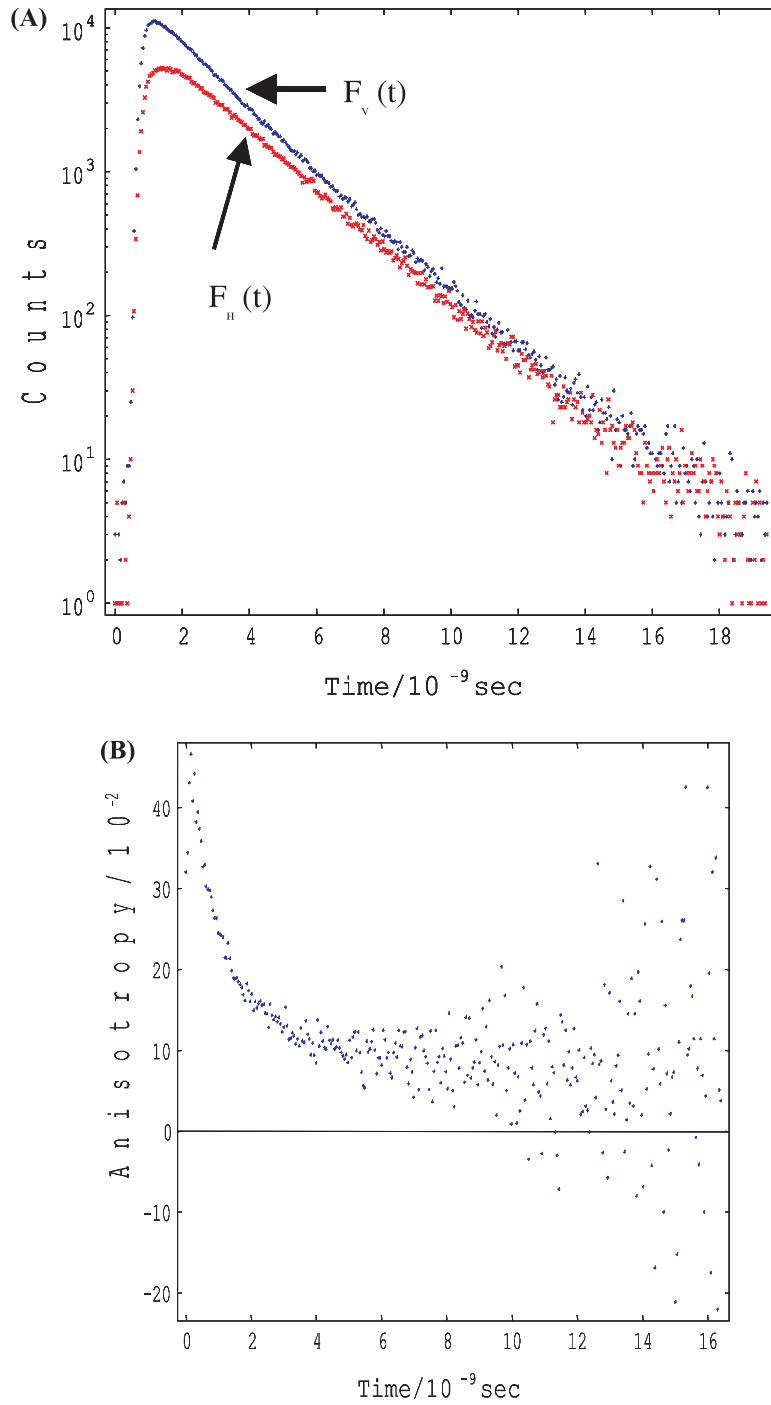
Fig. 4. Typical vertically, $F_V(t)$, and horizontally, $F_H(t)$, polarised fluorescence decay curves (A) and the derived anisotropy decay (B).

Table 2
Kinetic analysis of a 12.70% SiO_2, 0.25 N sol–gel, using Eqs. (2), (5) and (4)/(6)

Time	Fitting to Eq. (2)			Fitting to Eq. (5)				Fitting to Eqs. (4) and (6)			
	τ_r (s)	R_0	χ^2	τ_{r1} (s)	τ_{r2} (s)	R_0	χ^2	τ_r (s)	R_0	R_∞, (fR_0)	χ^2
17.5	$7.71e^{-9}$	0.299	2.95	$6.92e^{-10}$	$1.34e^{-8}$	0.375	1.02	$1.98e^{-9}$	0.342	0.131	1.33
28	$9.56e^{-9}$	0.308	2.91	$5.63e^{-10}$	$1.56e^{-8}$	0.389	1.18	$2.15e^{-9}$	0.345	0.154	1.62
36	$1.27e^{-8}$	0.306	2.73	$7.82e^{-10}$	$1.99e^{-8}$	0.371	1.09	$2.39e^{-9}$	0.344	0.167	1.39
48	$1.37e^{-8}$	0.307	2.60	$8.16e^{-10}$	$2.32e^{-8}$	0.366	1.06	$2.35e^{-9}$	0.342	0.178	1.30
57.5	$1.46e^{-8}$	0.313	2.25	$5.52e^{-10}$	$2.16e^{-8}$	0.380	1.06	$2.66e^{-9}$	0.342	0.186	1.39
70	$1.72e^{-8}$	0.313	2.44	$6.69e^{-10}$	$2.62e^{-8}$	0.375	1.10	$2.44e^{-9}$	0.346	0.199	1.39
78	$1.94e^{-8}$	0.312	2.31	$5.55e^{-10}$	$2.57e^{-8}$	0.380	1.02	$2.72e^{-9}$	0.344	0.201	1.37
88.5	$2.15e^{-8}$	0.314	2.07	$5.30e^{-10}$	$2.71e^{-8}$	0.376	1.00	$3.13e^{-9}$	0.340	0.205	1.43
109	$2.33e^{-8}$	0.312	2.09	$5.39e^{-10}$	$3.21e^{-8}$	0.372	1.05	$2.72e^{-9}$	0.339	0.218	1.35
125	$2.41e^{-8}$	0.318	1.82	$5.56e^{-10}$	$3.63e^{-8}$	0.371	0.97	$2.71e^{-9}$	0.341	0.229	1.22
133.5	$2.43e^{-8}$	0.322	1.86	$7.25e^{-10}$	$3.81e^{-8}$	0.365	1.09	$2.87e^{-9}$	0.344	0.231	1.31
165	$3.31e^{-8}$	0.319	1.96	$5.37e^{-10}$	$4.60e^{-8}$	0.371	1.16	$2.51e^{-9}$	0.343	0.248	1.33
265	$4.09e^{-8}$	0.325	1.43	$5.28e^{-10}$	$6.30e^{-8}$	0.363	0.97	$2.75e^{-9}$	0.341	0.268	1.13
278	$4.55e^{-8}$	0.324	1.56	$2.73e^{-10}$	$5.90e^{-8}$	0.386	1.07	$2.77e^{-9}$	0.340	0.271	1.32
305.5	$5.15e^{-8}$	0.326	1.55	$5.77e^{-10}$	$7.65e^{-8}$	0.361	1.11	$2.35e^{-9}$	0.344	0.279	1.24
370.5	$5.29e^{-8}$	0.327	1.55	$3.99e^{-10}$	$6.87e^{-8}$	0.368	1.17	$2.94e^{-9}$	0.341	0.278	1.38
1709.5	$9.96e^{-8}$	0.361	1.01	$1.52e^{-10}$	$1.19e^{-7}$	0.410	0.93	$1.07e^{-8}$	0.363	0.304	1.00
2991.5	$1.01e^{-7}$	0.374	1.05	$5.09e^{-11}$	$1.10e^{-7}$	0.464	1.00	$1.77e^{-8}$	0.376	0.290	1.04
4223	$7.15e^{-8}$	0.326	1.19	$5.39e^{-10}$	$7.82e^{-8}$	0.339	1.13	$1.90e^{-8}$	0.328	0.215	1.18
7250	$7.59e^{-8}$	0.375	1.11	$5.36e^{-10}$	$8.31e^{-8}$	0.386	1.09	$3.02e^{-8}$	0.376	0.204	1.10
8860	$6.82e^{-8}$	0.367	1.04	$5.34e^{-10}$	$7.28e^{-8}$	0.378	1.02	$2.52e^{-8}$	0.369	0.206	1.04
9975	$6.91e^{-8}$	0.336	1.14	$1.02e^{-10}$	$7.21e^{-8}$	0.393	1.04	$2.07e^{-6}$	0.336	-9.504	1.14
13011	$6.66e^{-8}$	0.349	1.07	$5.25e^{-10}$	$7.05e^{-8}$	0.360	1.04	$4.18e^{-7}$	0.349	-1.800	1.07

parameters such as a negative residual anisotropy were obtained. This implies that fluorescence from dye bound within the gel matrix is negligible in comparison to that from free dye within the sol and dye bound to silica particles. On the basis that Eq. (5) provides the best description of the probe dynamics we turn now to its interpretation. Firstly, it is important to note that precipitating out the silica at various times during the sol to gel transition, by the addition of methanol, revealed the probe to be both free in solution and attached to silica with more dye recovered in the methanol filtrate at earlier times. This fact alone suggests that the fluorescence anisotropy data reflect the joint contributions of solvated unbound probe molecules rotating in the fluid and probe molecules bound to silica particles. As we will explain, the self-consistent nature of all the parameters derived from Eq. (5) bears out this interpretation.

We can see from Table 2 that Eq. (5) provides R_0 values closest to the theoretical maximum of 0.4 and which are reassuringly constant as the fractional contribution to the total fluorescence from dye bound to silica particles, f, varies. Fig. 5 shows f for System a increasing with silicate concentration and duration of polymerisation and which can be modelled according to

$$f \approx f_0 + (f_{max} - f_0)(1 - e^{-ct}), \tag{13}$$

where $c \approx 10^{-4}$ s^{-1}. The modelling necessity for $f_0 \neq 0$ probably just reflects the non-diffusion controlled take-up of the dye at $t = 0$, although clearly in reality, $f_0 = 0$.

Similar trends are reproduced for System b at constant silicate concentration and varying acid normality. Fig. 5 explains why at long times Eq. (2) gives quite a good fit to the anisotropy decay (cf. Table 2), since in this case nearly all the emission originates from dye bound to silica particles. We observed the total fluorescence count rate to increase during polymerisation (e.g., $\approx 30\%$ for 15.3% SiO$_2$ in Fig. 5) and this probably reflects an increase in fluorescence quantum yield when the dye is bound to silica. For this reason Fig. 5 probably overestimates the actual fraction of the total number of probe molecules which are bound to silica. The fraction f is also influenced by whether or not the binding energy of the probe to silica particles is the same in the ground and excited states, but this has no effect on our hydrodynamic interpretation. It is worth recounting that in previous work on alcogels of tetramethyl orthosilicate [5], no change in the fractional contributions of the two rotational times was observed until well after t_g and the onset of syneresis.

Fortunately, the fluorescence lifetime of JA120 shows little variation between water and silica (the mean lifetime increasing from 2.38 ns at the outset
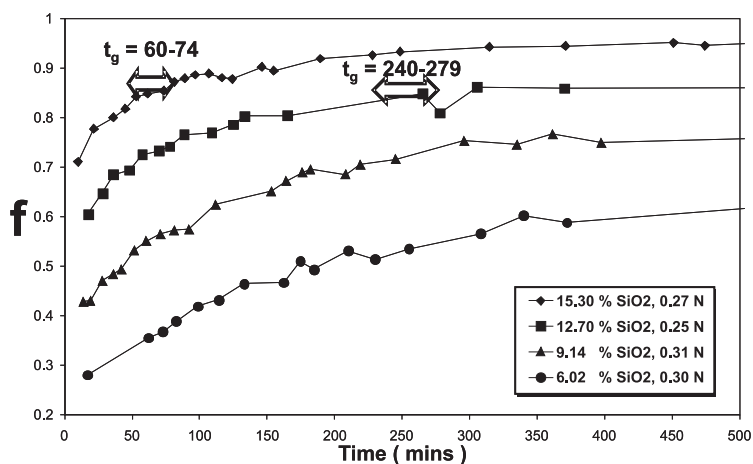

Fig. 5. The fraction f of total fluorescence due to dye binding to silica particles vs. time for System a sol–gels of varying silicate concentration and constant excess acid normality.

to 2.86 ns at the end for the System a sol of 15.30% SiO_2 and 0.27 N) so the anisotropy analysis is simplified in this respect. Certainly none of the anisotropy decay curves we have measured pass through a minimum, which would be indicative of heterogeneous environments with a significant difference in fluorescence lifetime [12]. The question then arises as to whether or not we can determine rotational times as long as 20–100 ns with such a short fluorescence lifetime. Prior to this work our first reaction would have been to think not. However, the monotonic change in τ_{r2} with time and better fit to Eq. (5) over all the eight compositions studied give us some confidence in this interpretation. The fractional increase with time of fluorescence associated with the longer rotational component helps us in this.

Turning now to the rotational correlation times determined with Eq. (5), it is a striking feature of Table 2, and indeed all our measurements, how τ_{r1} is fairly constant within the range $\approx$0.5–1 ns and this constancy within the error is illustrated in Fig. 6 for the corresponding microviscosity, derived from Eq. (3) to be in the range 1–2 cp. We

associate τ_{r1} with the rotation of the probe in the fluid part of the sol and indeed in residual fluid in the gel. Hence the microviscosity is significantly less than the bulk viscosity at all times. Although the errors are quite large, the small change in τ_{r1} across the macrogelation point is a common feature of all the compositions studied. Hence, despite the large errors there is also some evidence in our data that the microviscosity is lowered slightly after gelation and this would be consistent with loss of low molecular weight silicate species from the fluid. A microdomain of constant microviscosity of $\approx$2 cp coexisting with higher viscosity microdomain, which increased in microviscosity from $\approx$10 to 1000 cp during polymerisation, was proposed in previous work on alcogels [5]. Our interpretation of the anisotropy decay in hydrogels differs from this mainly in that we account for the slower depolarisation component in terms of the dye binding to silica particles.

5. Discussion

At present it is unclear as to whether or not the differences between our findings for acidic hydrogels and those reported for tetramethyl orthosilicate using rhodamine 6G as a probe in the pH range 4–8 [5] can be attributed to fundamental differences in the sol–gel processes, the influence of pH or the differing probes used. In our opinion, it seems that the presence of silica particles from very early on is consistent with all of our findings and some of the data reported on alcogels by Bright et al. [5]. Like JA120, rhodamine 6G is a xanthene probe capable of binding to silica particles. Moreover, numerous techniques have revealed evidence in silicon alkoxide sols for the formation of primary particles of $\approx$1–2 nm diameter, which then aggregate to form secondary particles up to $\approx$6 nm diameter, linkage of the latter in three dimensions then leading to gelation [13–16].

It is interesting to speculate on the binding mechanism of JA120 to silica particles. Given that JA120 is cationic it might be expected to readily bind to silica particles at a pH > 2, but in the pH range we are operating of 0.1–1 the surface charge on silica particles is slightly positive. Nevertheless
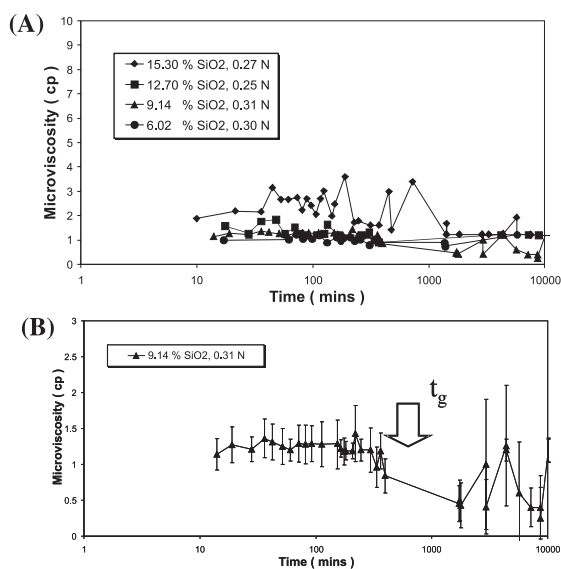

Fig. 6. Fluid microviscosity vs. time for System a sol–gels of varying silicate concentration and constant excess acid normality (A), with the error bars shown for one of the sets of data (B).

such mutual repulsion does not eliminate particle aggregation, but merely leads to reaction limited cluster–cluster aggregation [1]. Indeed the condensation binding mechanism between silica particles (Eq. (10)) may well be applicable to JA120 via its carboxylic acid functional group. The dye probably intercalates quite fully since there is no evidence of wobbling in a cone depolarisation as well [9], which might lead to an anisotropy decay described by three rotational times or two rotational times as well as a residual anisotropy.

We have observed identical trends to those reported here for another probe, JA53, which has a similar structure, but is somewhat smaller than JA120 and has a hydrodynamic radius of 6 Å. It is also worth noting that the absorption spectrum of JA120 and JA53 remain constant throughout the polymerisation. This means that we can exclude the possibility of dye–dye aggregation accounting for the longer rotational correlation time.

Hence, we associate the longer rotational time with that of dye binding to extremely small silica particles, which either exist initially or are formed soon after mixing. From this we are able to determine from Eq. (3) a maximum size of the particles which are present within 20 min of initial mixing as having a mean radius of ≈ 1.5 nm. 'Maximum' because we have made no allowance for the dimensions of the dye (≈ 0.7 nm, although it may well intercalate) and the possibility of water molecules being associated with the silica. As such, our fluorescence evidence for small silica particles being present very early in the gelation process provides complementary information from a new direction to what was thought to be the case from data obtained using other techniques.

The primary particle radius of ≈ 1.5 nm which we observe from the decay of fluorescence anisotropy is in close agreement with values reported from small angle scattering measurements made in many different laboratories over a range of sol–gel samples. For example, light scattering measurements on a silicon alkoxide sol found a primary particle hydrodynamic diameter of 1.0 nm increasing to 2.4 nm prior to gelation [13]. Small angle X-ray scattering studies of silica gel have revealed evidence for 1 nm particles [14] and similar studies on another alkoxide sol indicate that 2

nm diameter primary particles aggregate to form secondary particles of 6 nm diameter prior to gelation [15]. Small angle neutron scattering has produced comparable primary particle dimensions [16]. In one of the few studies on silica hydrogel formation, primary particles of ≈ 1 nm have been detected using small angle X-ray scattering [17].

Figs. 7 and 8 show how the mean particle size changes from the outset for Systems a and b,
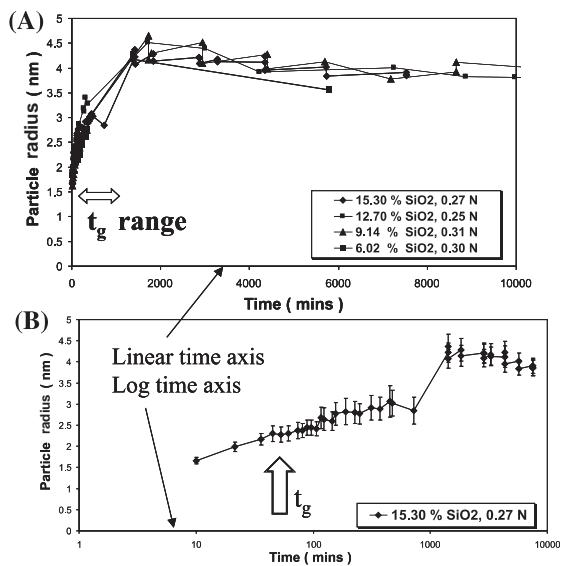

Fig. 7. Particle mean radius vs. time for System a sol–gels of varying silicate concentration and constant excess acid normality (A), with the error bars and t_g shown for one of the sets of data (B).
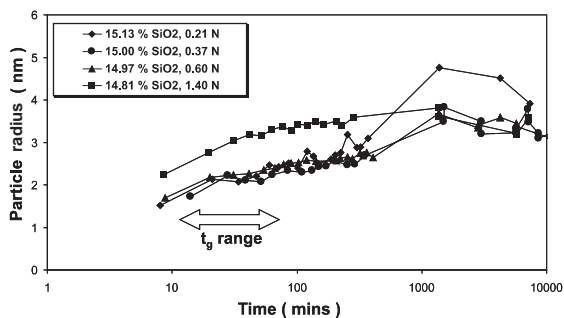

Fig. 8. Particle mean radius vs. time for System b sol–gels of constant silicate concentration and varying excess acid normality.

respectively. From τ_{r1} we have calculated two mean viscosities in the temporal regions where they prevail for each sol (see Fig. 6) and hence determined particle diameters using Eq. (3).

At moderate acidities (pH 0–2) the solubility of silica is quite low and silicate species are not thought to be highly ionised [1]. For these reasons it is likely that the formation and aggregation of primary particles occurs together and Ostwald ripening [1] (the process by which small particles dissolve and large ones grow because of their solubility differences) contributes little to growth after particle sizes exceed 1.5–2.0 nm diameter. Hence developing gel networks at moderate acidities are thought to be composed of small primary particles which link through siloxane polymerisation. Indeed, up to pH 7 [1] all the experimental evidence points to primary particle aggregation leading to clusters of mean diameter $\leqslant 6$ nm [13–17]. At pH > 7 primary particles are sufficiently anionic for Ostwald ripening to be the dominant growth mechanism, with much larger particle diameters ($\geqslant 100$ nm) being possible.

The initial aggregate growth shown in Figs. 7 and 8 can be well described to a first order approximation (linear regression coefficient $R^2 \sim 0.96$) by a function of the form

$$r = r_0 + (r_{max} - r_0)(1 - e^{-kt}), \tag{14}$$

where the initial radius r_0 ranges from 1.4 to 1.7 nm (uncorrelated with [SiO_2]). For Fig. 7 (constant pH of $\approx$0.8–0.9 and varying silicate concentration) the rate parameter k is $\approx 3.3 \times 10^{-5}$, 6.0×10^{-5}, 8.6×10^{-5} and 1.7×10^{-4} s^{-1} for a 6.02% (weight for weight), 9.14%, 12.7% and 15.3% SiO_2, respectively. For Fig. 8 (constant silicate concentration of $\approx$15% and varying pH) the k values are $\approx 1.9 \times 10^{-4}$, 1.9×10^{-4}, 3.9×10^{-4} and 6.8×10^{-4} s^{-1} for a pH of 0.98, 0.73, 0.52 and 0.15, respectively. (Because the rise times are faster we have shown the time axis in Fig. 8 on a log scale.) The reaction probability for particle aggregation might be expected to be reduced as the surface positive charge increases and the solubility of silica is known to decrease with decreasing pH. These facts seem to be reflected in the smaller maximum particle radius of Fig. 8 at pH $\leqslant 0.73$ ($\approx$3.5 nm) as compared to that at higher pH shown in Fig. 7

($\approx$4.5 nm). Simple geometry considerations predict that a three-fold increase in particle diameter corresponds to an aggregate containing a maximum of $\approx$13 primary particles [18]. For the particle growth parts of both Figs. 7 and 8 we have been able to resolve $\approx$10 monotonically increasing data points spanning 1 nm, suggesting that our resolution is close to 1 Å.

Perhaps the most striking feature of Fig. 7, and to a lesser extent Fig. 8, is the manner in which the mean particle radius increases to a peak and then decreases slightly by $\approx$0.5 nm as synersis occurs and water evaporates from the gel. Unsealed cuvettes containing silica hydrogels typically show a 40% loss in weight due to water evaporation after one week from preparation. Hence it would be prudent to acknowledge the possibility that if the dye is not readily taken up within the gel the apparent decrease in particle size might be an anomalous result caused by depolarisation due to dye–dye Förster non-radiative resonance energy transfer as the dye aggregates. Unfortunately, attempts to analyse the fluorescence decay in terms of Förster resonance energy transfer [9] proved to be inconclusive due to the presence of a weak ($\approx$4% of the total fluorescence), but fast decay component ($\approx$1.5 ns) from JA120 [11] (taken account of in the anisotropy analysis [9]). Nevertheless, the observation that the maximum particle size occurs after the t_g of most of the sols might argue against depolarisation due to dye aggregation. Also, throughout the polymerisation process we have found no change in absorption spectrum of the dye as would be indicative of dye clustering. Moreover, the rate of decay of anisotropy is constant after $\approx$6000 min, despite the gel drying and this is inconsistent with Förster resonance energy transfer. Scattering of fluorescence at multiple sites can lead to anisotropy decay, but again, in this case we would not expect the decay of anisotropy to level off after 6000 min. Particle size reduction due to re-dissolution of silica seems unlikely at such a low pH. Sieve deposition of larger particles in the gel or reduction in the hydration sphere also seems unlikely. Hence we propose that the size decrease we observe reflects the dominance of intra-particle synersis over further aggregation at later times.

Syneresis is a term more usually applied to gels, but at the molecular level it involves, in the simplest form, shrinkage via conversion of monosilicic acid, $Si(OH)_4$, to siloxane (–Si–O–Si–) bridging bonds through polycondensation reactions (Eq. (10)). Primary particle syneresis probably occurs from the outset, but is offset at earlier times by the much greater aggregation rate (the condensation rate is minimised at close to the isoelectric point [1]). The aggregation rate would be expected to slow down as the number of particles decrease and the rate of particle syneresis slows down as all but the sterically hindered condensation sites are used up. Just prior to r_{max} the net k value might be expected to reduce by syneresis. Figs. 7 and 8 show all these features. From Fig. 7 the particle syneresis rate constant, assuming an exponential reduction in particle radius and that growth is absent after 30 h, is $\approx 6.0 \times 10^{-6}$ s^{-1}, i.e., at least an order of magnitude lower than the typical growth due to aggregation which we observe. Particle syneresis is seen to be effectively over after ~100 h.

Finally, it is interesting to compare the shape of the particle growth parts of Figs. 7 and 8 with recent electron microscopy studies of sols produced from base catalysed tetraethyl orthosilicate (TEOS) [19]. This study [19] revealed aggregate growth starting from ≈ 100 nm particle diameter which, like our data on nm primary particles, is well described by Eq. (14).

6. Conclusions

The picture emerging of the sol–gel process in silica hydrogels is one of siloxane polymerisation leading to aggregation of ≈ 1.5 nm primary particles to form ≈ 3.5–4.5 nm secondary particles, irrespective of the sol or the time taken for macrogelation. The fluid present in the sol is depleted of silicate as polymerisation proceeds and this process continues after the point of macrogelation is reached and water is expelled from pores as the gel shrinks under the action of syneresis. The microviscosity of the fluid, whilst never departing far from that of water during the whole process, converges to that of water towards the

end. This is in stark contrast to the massive increase in bulk viscosity preceding the gel point. To the best of our knowledge intra-particle syneresis has not previously been reported using conventional techniques such as small angle X-ray scattering. The effect of intra-particle syneresis on particle dynamics calculations and the final gel are interesting topics and worthy of further consideration in future work.

As Figs. 7 and 8 show the technique we have developed approaches Å resolution, it is relatively inexpensive and suitable for in situ studies even at high silicate concentration and well beyond the t_g. It could be easily adapted for on-line monitoring of sol–gel production in a manufacturing plant and should also be suitable for studying other colloids, e.g., TiO_2. Further development might also lead to the measurement of size distributions both in the silicate liquor and sol. The approach is limited in its application only by the dye–particle interaction; the upper limit of particle size measurement being determined by the dye fluorescence or phosphorescence lifetime and the lower limit by the dye hydrodynamic diameter.

In a more general context, our interpretation of the time-resolved fluorescence anisotropy in silica hydrogels also provides a means of separating the behaviour of both free and bound dye. This may well offer a general approach to the problem of monitoring molecular adsorption in related areas, e.g., protein take-up by silica particles used in fining applications.

References

[1] C.J. Brinker, G. Scherer, Sol–Gel Science, The Physics and Chemistry of Sol–Gel processing, Academic Press, San Diego, CA, 1989.

[2] R. Reisfeld, J. Non-Cryst. Solids 121 (1990) 54.

[3] J.R. Lakowicz, Ed., Topics in Fluorescence Spectroscopy, vols. 1, 2, 3 and 4, Plenum, New York, 1991, 1991, 1992 and 1994, respectively.

[4] B. Dunn, J.I. Zink, J. Mater. Chem. 1 (6) (1991) 903.

[5] F.V. Bright, U. Narang, R. Wang, P.N. Prasad, J. Phys. Chem. 98 (1994) 17.

[6] K.H. Drexhage, N.J. Marx, J. Arden-Jacob, J. Fluorescence 7 (1, Suppl.) (1997) 91s.

[7] I. Soutar, in: N.S. Allen (Ed.), Developments in Polymer Photochemistry – 3, Applied Science, Barking, p. 125 (Chapter 4).

[8] M.R. Eftink, in: C.H. Suelter (Ed.), Methods of Biochemical Analysis, vol. 35, Wiley, 1991, p. 127.

[9] D.J.S. Birch, R.E. Imhof, in: J.R. Lakowicz (Ed.), Topics in Fluorescence Spectroscopy, vol. 1, Plenum, New York, 1991, p. 1 (Chapter 1).

[10] D.A. Hatrick, PhD thesis, Strathclyde University, 1997.

[11] C.D. Geddes, J.M. Chevers, D.J.S. Birch, J. Fluoresc. 9 (1999) 73.

[12] R.D. Ludescher, L. Peting, S. Hudson, B. Hudson, Biophys. Chem. 28 (1987) 59.

[13] A.H. Boonstra, T.P.M. Meeuwsen, J.M.E. Baken, G.V.A. Aben, J. Non-Cryst. Solids 109 (1989) 153.

[14] B. Himmel, Th. Gerber, H. Bürger, J. Non-Cryst. Solids 91 (1987) 122.

[15] G. Orcel, L.L. Hench, I. Artaki, J. Jonas, T.W. Zerda, J. Non-Cryst. Solids 105 (1988) 223.

[16] R. Winter, D.-W. Hua, P. Thiyagarajan, J. Jonas, J. Non-Cryst. Solids 108 (1989) 137.

[17] Th. Gerber, B. Himmel, C. Hübert, J. Non-Cryst. Solids 175 (1994) 160.

[18] D.E.G. Williams, J. Non-Cryst. Solids 86 (1986) 1.

[19] G.H. Bogush, C.F. Zukoski IV, J. Colloid Interf. Sci. 142 (1991) 1.